SIMBI, D. J., DINGWIZA, M., and BARKER, B. D. Influence of stress and electrochemical effects on initiation and morphology of pits in stainless steels exposed to an aqueous solution of boiling magnesium chloride. *INFACON 6. Proceedings of the 1st International Chromium Steel and Alloys Congress, Cape Town.* Volume 2. Johannesburg, SAIMM, 1992. pp. 165-171.

Influence of Stress and Electrochemical Effects on Initiation and Morphology of Pits in Stainless Steels Exposed to an Aqueous Solution of Boiling Magnesium Chloride

D. J. SIMBI*, M. DINGWIZA†, and B. D. BARKER‡
**University of Zimbabwe, Harare, Zimbabwe*
†Zimbabwe Iron & Steel Company, Redcliff, Zimbabwe
‡Department of Chemistry, Portsmouth Polytechnic, Portsmouth, UK

The role of stress and electrochemical effects in the nucleation and morphology of pits was investigated in two commercial-grade iron-based alloys, namely austenitic and ferritic stainless steels. Anodic polarization of looped specimens at varying potentials more noble to the pitting potential in an aqueous solution of 42 per cent boiling magnesium chloride induced severe pitting along the highly stressed parts of the looped specimen. Pit depths were found to increase with increasing polarization time for a given applied potential and physical state of the metal.

An examination of the pits by SEM indicated that pits formed in the austenitic steel were saucer-shaped, while those formed in the ferritic steel were slightly oval. A common feature observed in cold-worked austenitic steels was the occurrence of 'tracking' along the stressed portions of the looped specimen.

Unlike the austenitic type, the ferritic specimens were characterized by severe pitting of the edges. The corrosion product at the bottom of the pit showed a high concentration of metal and chloride species, suggesting their participation in the pitting process.

Introduction

Almost all the iron-based alloys referred to as stainless steels are susceptible to localized corrosion when exposed to chloride environments. This form of corrosion damage represents a limitation to the safe and reliable use of this complex group of alloys as construction materials in a number of industries. In the chemical and processing industries, for example, pitting corrosion is a major cause of repeated service failures[1]. The most important practical problem relates to austenitic stainless steels and to some of the more recently developed ferritic stainless steels[2,3]. The unanticipated occurrence and unpredictable rate of pit propagation make it difficult for engineers to allow for the phenomenon of pitting corrosion when considering practical engineering designs.

Metal damage by pitting corrosion is characterized by a marked difference between the rate of metal dissolution in the pits and that on the passive surface. While the metal is estimated to corrode in the passive state at a rate approximating 10^{-6} A·cm^{-2}, dissolution in the pits can reach up to 10 A·cm^{-2}. This results in intensive localized corrosion attack, which quickly leads to the deterioration and destruction of materials and structures.

The pitting corrosion of stainless steels has been widely reported in a number of investigations[4-13]. These studies have indicated that the breakdown of the passive surface film that leads to pitting corrosion may arise from a combination of mechanical, metallurgical, environmental, and electrochemical effects. Impact by particles flowing in corrosive media may, for example, cause the initial breakdown of the passive film, leading to either pitting or an impingement corrosion attack. The former is considered to be a special form of crevice corrosion since pits that develop constitute a self-perpetuating region of localized corrosion. Mechanical stresses within the metal may manifest themselves in other localized forms of corrosion damage, notably hydrogen embrittlement and corrosion fatigue phenomena.

Predicting pitting corrosion is extremely difficult, particularly as the complexity of the corrosive environments increases, and even more so when fluctuations occur in the environmental parameters and internal stress state of the metal, as often arise in process plant. The present study is an investigation of the influence of stress and electrochemical effects on the nucleation and morphology of pits formed in ferritic and austenitic stainless steels exposed to a boiling aqueous solution of magnesium chloride. This corrodent has been widely used to determine the susceptibility to stress–corrosion cracking of stainless steels.

Materials

Samples of commercial-grade ferritic (430S15) and austenitic (304S15) stainless steel supplied in sheet form

(0,85 mm thick) were used in this investigation. The chemical composition of the steels is given in Table I.

TABLE I
CHEMICAL COMPOSITION OF TWO COMMERCIAL-GRADE STAINLESS STEELS (IN PERCENTAGES)

Grade	C	Cr	Ni	Mn	Si	S	P
304S15	0,06	18,2	10,5	0,90	0,19	0,03	0,04
430S15	0,10	17,5	0,50	1,00	0,80	0,03	0,04

The test solution used was prepared from reagent-grade magnesium chloride and demineralized water. Dilute aqueous solutions of sodium hydroxide and hydrochloric acid were used to adjust the pH of the test solution to the desired value.

Experimental Procedure

Determination of E_{pit} from Polarization Curves

A Standard Potentiostat Wenking ST72 instrument was used in conjunction with a scanning potentiometer Wenking SMP69 to measure polarization curves in a solution of 42 per cent $MgCl_2$ for each of the stainless steels tested.

Samples for the determination of polarization curves were sheared from commercially available strip stock to give a total surface area of 1 cm^2. After they had been mounted in an inert cold-setting epoxy resin, the samples were polished to a 1 μm finish, degreased in ethanol, and hot-air dried. Platinum wire was used as the counter electrode, and a saturated calomel electrode with a double junction as the reference electrode. The working electrode was immersed in the test solution for 15 minutes, after which the potential scan was commenced from –1000 mV in the anodic direction, terminating the run at +200 mV. The corresponding current values were approximately 0,5 $mA{\cdot}cm^{-2}$ and 0,15 $mA{\cdot}cm^{-2}$ at pH 2 and 4, respectively. The stepping rate was 60 $mV{\cdot}min^{-1}$, the values of current and potential being plotted automatically on a Linseis recorder at a chart speed of 500 $mm{\cdot}h^{-1}$. The protection potential, E_{pp}, was estimated for each type of steel from where the hysteresis loop joined the potential–current curve on the reversal of the potential after E_{pit} had been reached. The results were used in an assessment of the potentiostatic conditions required to produce pitting in long-term exposure tests in boiling $MgCl_2$ solution.

Anodic Polarization of Looped Specimens

Specimens measuring 150 x 13 x 0,85 mm were prepared from strip material in stock, and were then stress relieved at 500 °C for 1 hour and furnace-cooled. The heat treatment accorded was necessary to remove stresses introduced by machining during the preparation of the specimens, particularly along the sheared edges. The specimens were then deformed plastically into the form of a loop, and the two ends were clamped together by plastic nuts and bolts before being placed into a holder and fitted into the corrosion test cell. The latter comprised a 0,25 dm^3 reaction vessel clamped with a spring-coiled wire to a multi-necked top, which was fitted with a reflux condenser. An electric heating mantle of 0,25 dm^3 capacity was used to heat the test solution to its boiling temperature.

The looped specimen was immersed in the test cell and polarized to pre-determined potential values ranging from below E_{pp} to just above E_{pit} for the stainless steel under test. All the tests were run for times ranging from 10 to 300 minutes under conditions of anodic polarization.

Measurement of Pit Depths

After each test run, the specimen was washed with distilled water, rinsed with ethanol, and hot-air dried. Segments approximately 10 x 10 mm were then cut from the test piece for measurement of pit depth by use of an M41

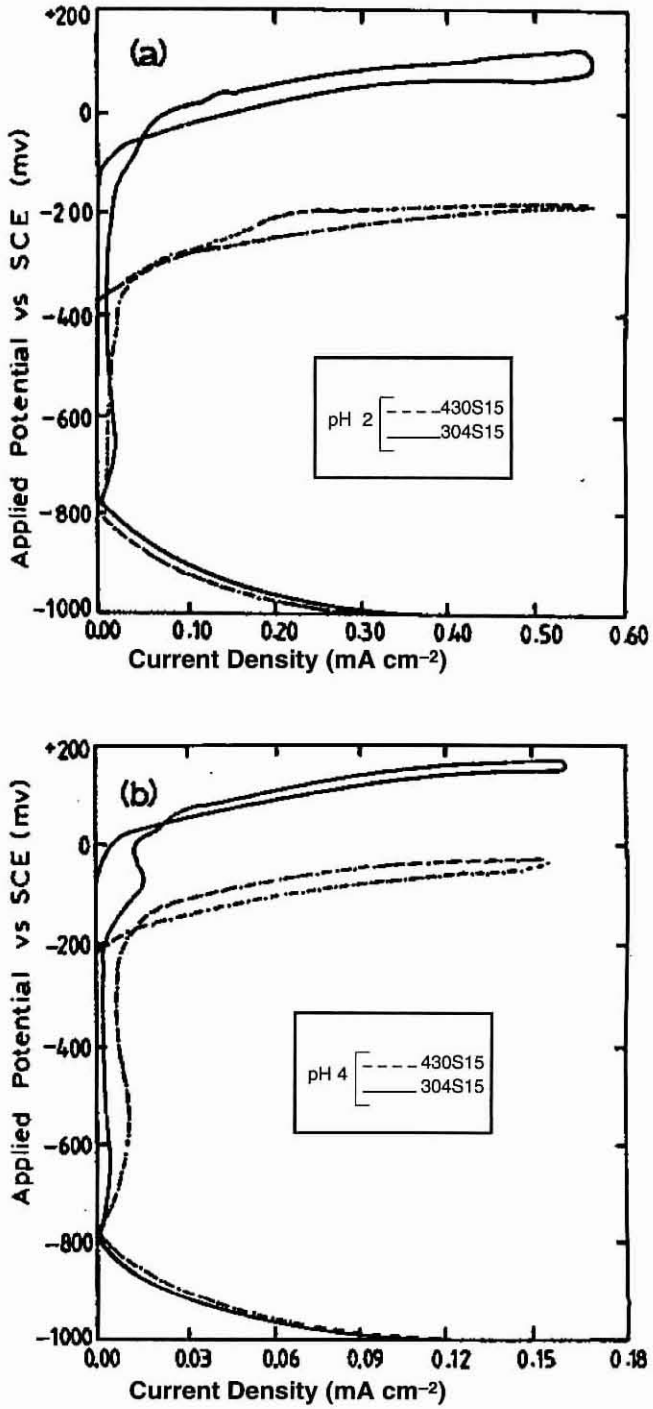

FIGURE 1. Polarization curves for two stainless steels at (a) pH 2 and (b) pH 4 in 42 per cent aqueous $MgCl_2$ solution at room temperature. The effect of the pH of the bulk solution on I_{pass} should be noted

Photon Microscope. This was carried out by initially focusing the instrument at the edge of the pit, noting the reading on the micrometer gauge, and then focusing at the bottom of the pit. The difference in the reading on the micrometer gauge gave pit depths in micrometres. The general shapes of the pits and their distribution were carefully noted.

SEM Examination of Pitted Samples

The same segments as were used for the measurement of pit depths were mounted on aluminium disks and examined for the presence of pits by use of a Cambridge Stereoscan 180 scanning electron microscope, which had a Links System facility for qualitative elemental analysis.

Experimental Results

Polarization Curves

The potential–current density plots for the ferritic and austenitic stainless steels in a 42 per cent aqueous solution of $MgCl_2$ at room temperature are shown in Figure 1. The plots indicate a general similarity in shape, with the active/passive transition being absent. The reversal of the potential sweep after E_{pit} had been exceeded showed little hysteresis. Generally, the onset of E_{pit} was found to be more active for the ferritic steel than for the austenitic type, irrespective of the pH value of the bulk solution.

Measurements of Pit Depths

The variation in the depths of the pits with applied potential is shown in Figure 2. There was a general increase in pit depth as the applied potential was increased in the noble direction. The onset of pitting varied with both the applied potential and the type of stainless steel. Deeper pits were measured in samples that had been polarized at the higher pH value than in the samples with the lower pH (Figure 3). The introduction of a scratch to the tip of the loop and cold-work resulted in a marginal increase in depths for both steels, with the ferritic steel (Figure 4) showing a more pronounced sensitivity than the austenitic steel (Figure 5).

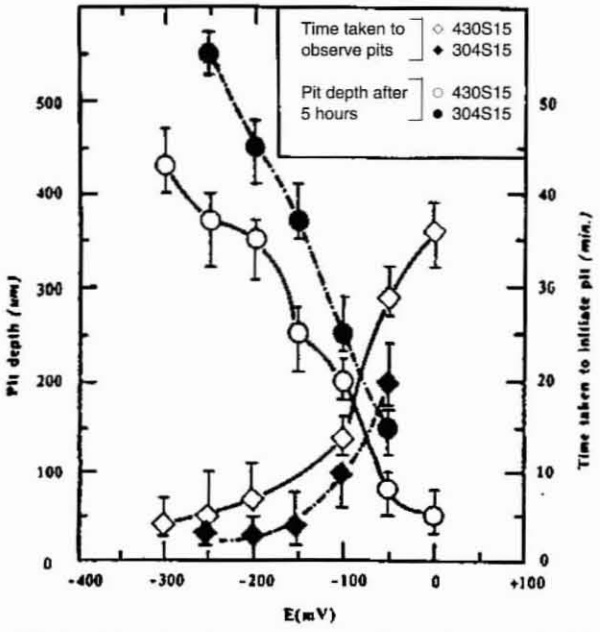

FIGURE 2. Effect of applied potential on maximum pit depth and minimum time for pits to be observed on ferritic and austenitic stainless steels exposed to a boiling aqueous solution of 42 per cent $MgCl_2$ under conditions of anodic polarization at pH 2

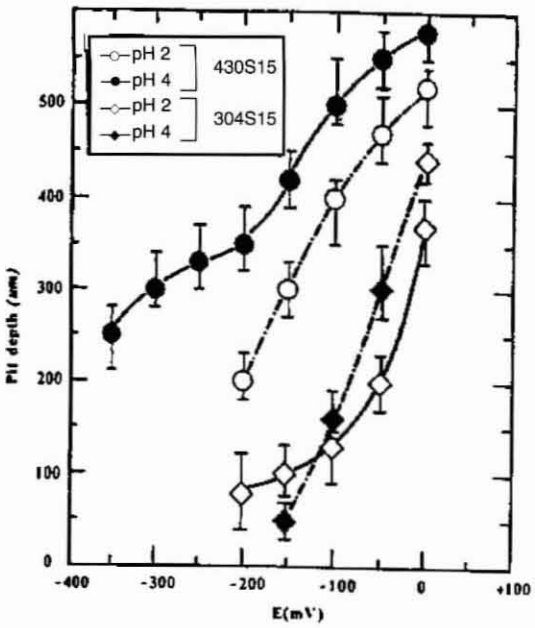

FIGURE 3. Effect of solution pH on maximum pit depth attained in ferritic and austenitic stainless steels exposed to a boiling aqueous solution of 42 per cent $MgCl_2$ under conditions of anodic polarization

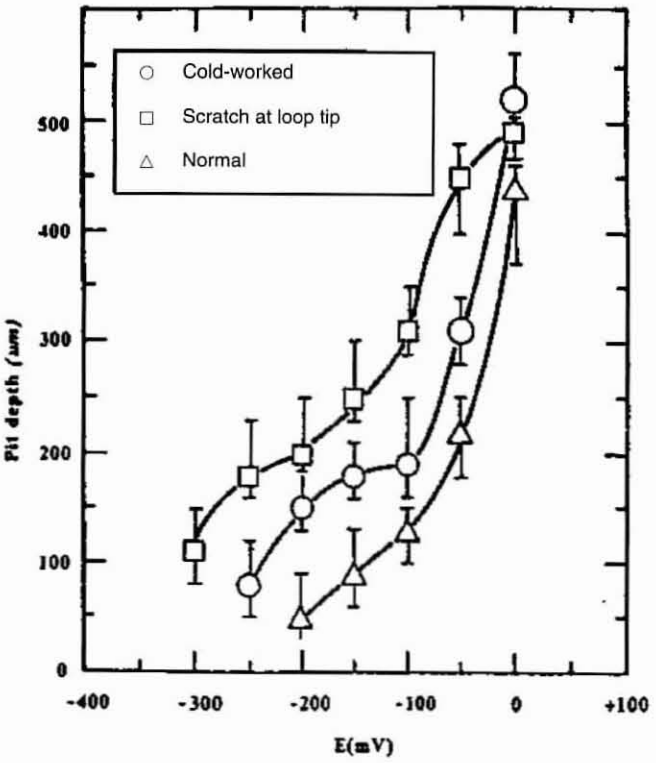

FIGURE 4. Effect of cold-work and scratching of specimen-loop tip on maximum pit depth in a ferritic stainless steel after 300 minutes of exposure to a boiling aqueous solution of 42 per cent $MgCl_2$ under conditions of anodic polarization at pH 2

The severity of pitting was determined from a comparison of the number of pits per square centimetre of area as

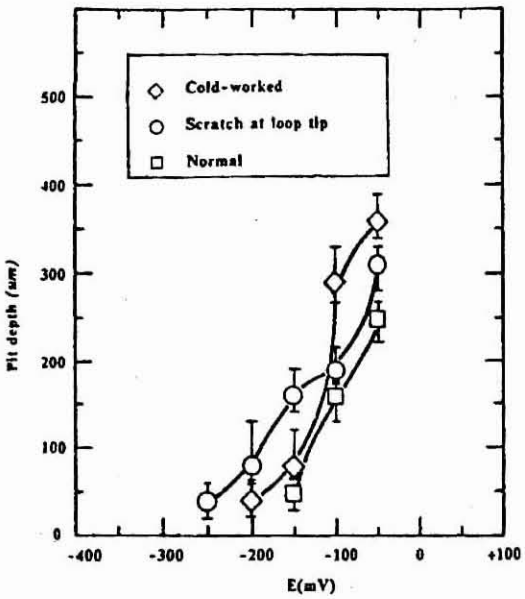

FIGURE 5. Effect of cold-work and scratching of specimen loop tip on maximum pit depth in an austenitic stainless steel after 300 minutes of exposure to a boiling aqueous solution of 42 per cent $MgCl_2$ under conditions of anodic polarization at pH 2

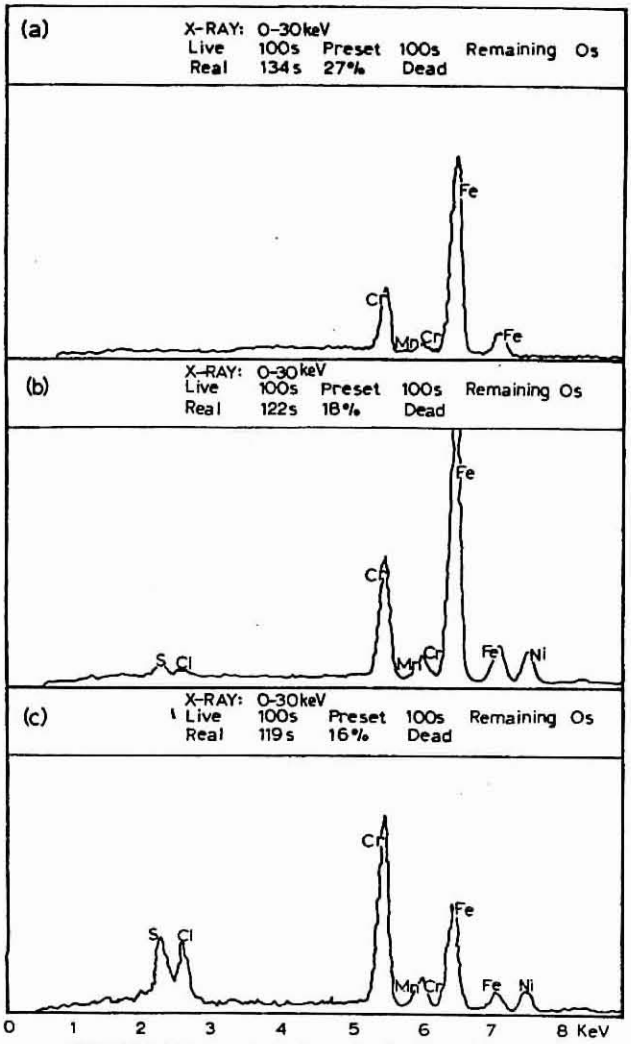

FIGURE 6. Microprobe analysis of a ferritic stainless steel
(a) Unpitted surface of an unexposed specimen
(b) Unpitted surface of an exposed specimen
(c) Corrosion products at the bottom of a pit

noted visually and by the use of an optical microscope. Generally, the density of the pits in the stressed areas and specimen edges was high, although most of them tended to be shallow, particularly in the austenitic steel. Severe pitting with perforation was observed in a number of specimens after 5 hours of exposure at potentials more noble than E_{pit}. The specimens of austenitic stainless steel exhibited 'tracking' along the stressed areas. Cold-working and scratching of the loop tip increased the pit density.

Analysis of the Corrosion Products

Sample sections were analysed for the elements present in pits or on unpitted surfaces. The results of this investigation indicated the presence of S and Cl species at the base of the pit. In addition to these, the alloying elements Cr and Ni were present in the pits (Figures 6 and 7). The height of the

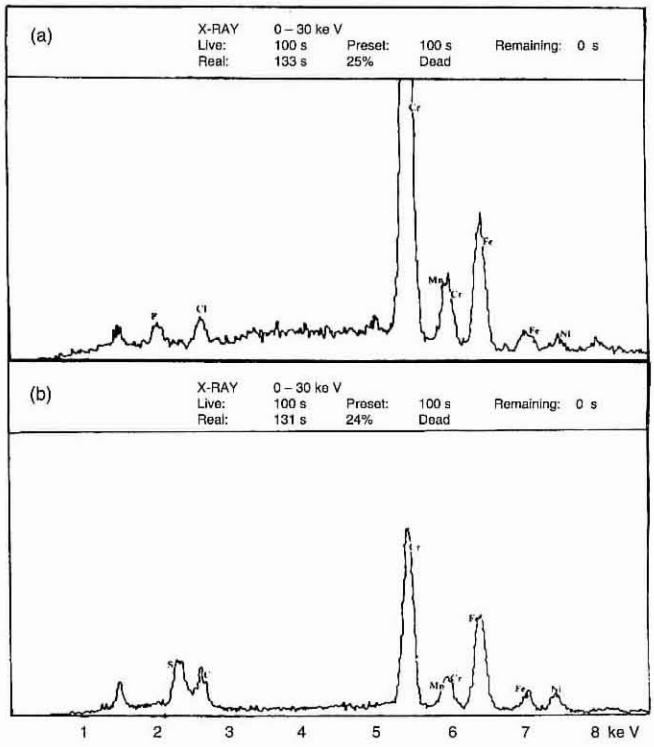

FIGURE 7. Microprobe analysis of an austenitic stainless steel
(a) Corrosion products at the bottom of a saucer-shaped pit
(b) Corrosion products in a pit formed in the scratched tip of a loop

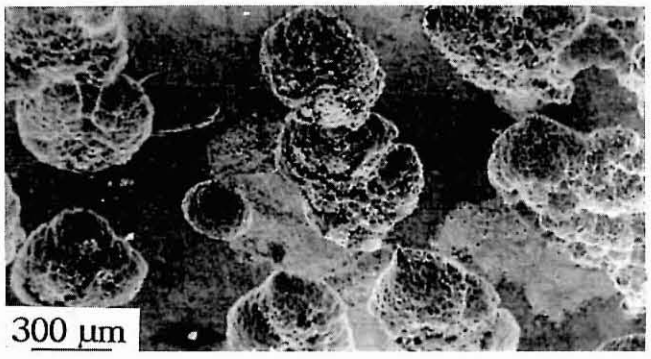

FIGURE 8. A specimen of austenitic stainless steel after 300 minutes of exposure in 42 per cent aqueous $MgCl_2$ solution at –100 mV applied potential, showing saucer-shaped pits. Pits growing near one another tended to merge, thereby forming large pits

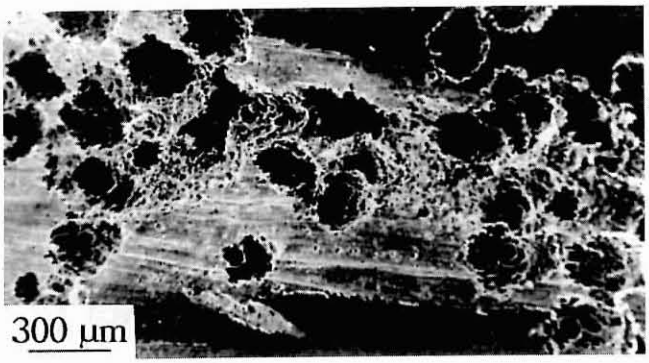

FIGURE 9. Saucer-shaped pits at a scratched loop tip of an austenitic stainless steel

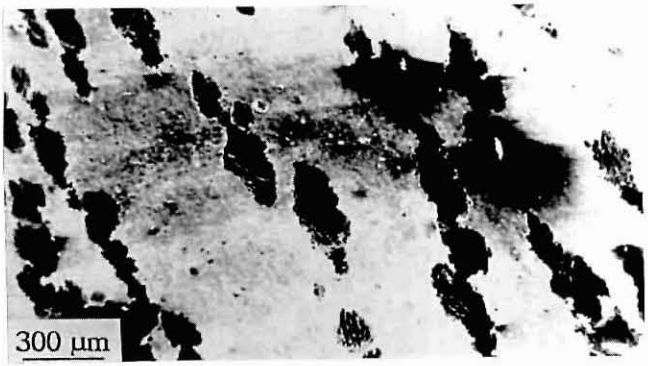

FIGURE 10. A speciment of ferritic stainless steel after 300 minutes of exposure in a boiling solution of 42 per cent aqueous $MgCl_2$ at –100 mV applied potential. The pits appear to be oval-shaped and are in rows

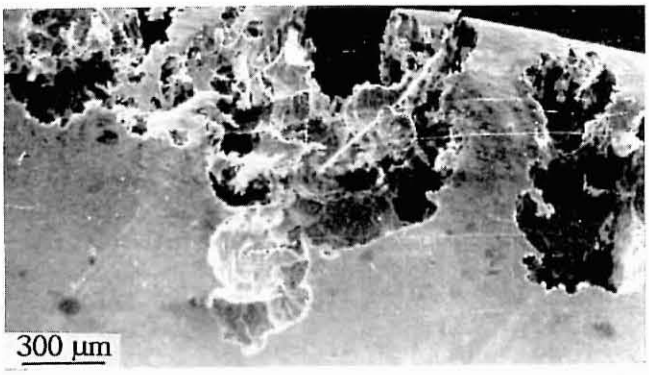

FIGURE 11. The edge of a severely pitted specimen in a cold-worked ferritic stainless steel after 300 minutes of exposure in a boiling aqueous solution of 42 per cent $MgCl_2$ at an applied potential of –50 mV

S and Cl peaks (Figures 6(c) and 7) suggests a higher concentration of these species in the pits than on the unpitted surfaces (Figures 6(a) and (b)). However, it is possible that the high Cr content measured in the pits could be due to preferential leaching of iron. A more sensitive technique such as Auger spectroscopy could have been more appropriate for the measurement of the passive layer composition.

Pit Morphology

Scanning electron micrographs of pitted ferritic and austenitic steels are shown in Figures 8 to 13. The saucer-shaped pits that were a common feature of the austenitic steel are displayed in Figure 8. The pits appeared to form close to one another and, as propagation proceeded, some

FIGURE 12. A cold-worked austenitic stainless steel showing tracking. The specimen was exposed to a boiling aqueous solution of 42 per cent $MgCl_2$ at an applied potential of –100 mV

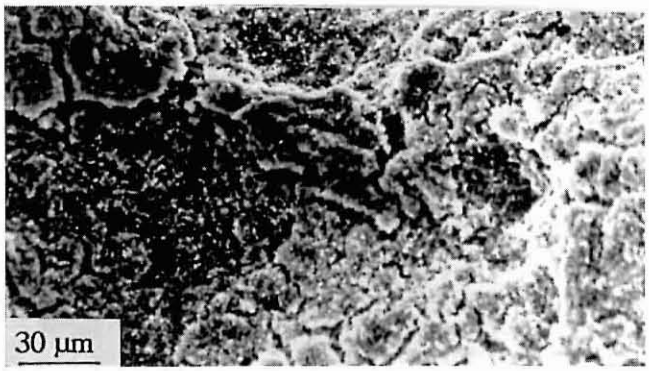

FIGURE 13. Corrosion products at the bottom of a saucer-shaped pit in an austenitic stainless steel

of them merged to form large pits. The pits tended to be shallow.

Severe pitting occurred in specimens with artificial scratches at the loop tip (Figure 9). The pitting of the ferritic stainless steel was characterized by oval-shaped pits that seemed to follow highly stressed areas (Figure 10). In addition, the pits formed along the edges of stressed specimens (Figure 11) tended to be very deep and sometimes perforated, compared with those observed in the austenitic steel. Some cold-worked austenitic specimens (Figure 12) exhibited 'tracking' along the highly stressed portions of the loop tip. Figure 13 shows corrosion products at the bottom of a pit in an austenitic steel.

Discussion

Examination of the relevant Pourbaix diagram for the metal–H_2O system for Cr indicates that the Cr_2O_3 phase is stable in solutions of neutral pH. In acid solutions of low pH, Cr would therefore be predicted to corrode. At pH values of 4 to 7 and more noble potentials, a zone of corrosion separates the regions of passivity and immunity. The disappearance of the active–passive transition in the polarization plots carried out in $MgCl_2$ solution can be attributed to immediate passivation of the steels by a surface film. This suggests the presence of a metastable film, which is not predicted by the potential–pH diagram since chromium is in the zone of corrosion. The metastable oxide will, however, dissolve slowly into the electrolyte. The current, I_{pass}, flowing is a measure of the dissolution rate of the metastable oxide and can be equated to the corrosion rate of the metal. From Figure 1 the measured I_{pass} for the ferritic and austenitic steels in 42 per cent $MgCl_2$ solution is an order of

magnitude higher at pH 2 than that at pH 4. When the potential is further increased in the noble direction, the passive–active transition, defined either as the transpassive potential, E_{tr}, or the pitting potential, E_{pit}, is reached. This is marked by a rise in the current density. Thus, the onset of E_{pit} appears to vary with the type of metal and the pH value of the corroding solution.

In investigations of anodic polarization, it was necessary to hold the potential of the stressed specimen at a value that would promote pit formation. While it might appear that this artificial polarization of the test piece would not truly represent a service condition, the test would serve to illustrate that the application of stress does influence the course of pitting corrosion. It has also been recognized that the pitting corrosion of metals in unstressed systems can occur only if the electrode potential is higher than E_{pit}. While, the pitting-potential ranges for each type of stainless steel were established from polarization runs in an aqueous solution of 42 per cent $MgCl_2$ at room temperature, the kinetics of the pitting-corrosion behaviour of the steels in this solution may alter considerably at elevated temperatures.

The susceptibility to pitting of stainless steels has been characterized by the presence of a hysteresis loop when the sweeping potential is reversed after attaining potentials more noble than E_{pit}. The presence of a critical pitting potential is supported by the results obtained from the anodic-polarization exposure tests. Below a certain applied potential, no pits were observed in either the ferritic or the austenitic stainless steel. Although the exact critical pitting potential was not determined, its value appeared to depend on the physical state of the specimen and the solution pH. It was also observed that, as the critical potential was reached in the active direction, the degree of pitting and the pit depths appeared to diminish. This suggests that, at E_{pit} and more active potentials, pits can neither nucleate nor can existing pits propagate. All active pit sites will thus immediately passivate below E_{pit}. As the applied potential was increased in the noble direction from E_{pit} to values immediately above it, the current flowing was observed to oscillate. In order to explain this observation, the existence of unstable pits is proposed. These are unstable in the sense that, once they are nucleated, they repassivate after some time at the same potential. At potentials more noble than E_{pit}, stable pits are initiated and will continue to grow at a steady rate at the same potential. The increased pit depths with perforations observed at potentials more noble than E_{pit} are thus explained. This also corresponds to the steady increase in current density with time after pit initiation.

The critical pitting potential is the minimum potential at which localized acidity can be maintained inside a pit, and the main reason for passivity breakdown is localized acidification due to hydrolysis of the metal ions. The exact nature of this process is not yet known, but it is envisaged as one involving the formation of aquocations of divalent or trivalent ions. As a result of the highly localized nature of the attack, chloride ions migrate into the pit nuclei to maintain neutrality. The analysis by microprobe of the corrosion products within some of the pits confirmed this hypothesis. Appreciable levels of chloride and chromium species were detected. The enrichment of chromium in the surface film indicates that the passive oxide film is mainly Cr_2O_3. Since nickel and manganese were identified, it can be assumed that the formation of aquocations involved these species as well.

The degree of pitting in both ferritic and austenitic stainless steels is influenced by the applied potential, as well as by the amount and location of induced stresses in the metal. Severe pitting, which was accompanied by perforations in some cases, occurred mainly along the highly stressed portions of the specimen loop. Pit nucleation and density were found to depend on residual stresses in the metal. In the austenitic steel, pit nucleation led to the formation of small clusters of pits that, on propagation, merged to form large ones. These pits tended to be shallow and saucer-shaped. Although the general morphology of the pit remained the same, the degree of pitting in specimens with a scratch at the loop tip and those which had been cold-worked was high, as indicated by the increased pit depth and density. The ferritic steel exhibited similar trends, the only difference being that the pits, which were oval in shape, tended to be much deeper than those in the austenitic steel.

Conclusions

(1) The onset of E_{pit} was found to be more active in the low-nickel ferritic stainless steel than in the austenitic type. However, both steels exhibited a small hysteresis on reversal of the potential sweep after E_{pit} had been exceeded.

(2) Measured pit depths were found to increase with exposure time as the applied potential was increased in the noble direction.

(3) Pitting was severe at highly stressed portions of the looped specimen, with scratching of the loop tip and cold-working of the specimen leading to increased pit density.

(4) The austenitic stainless steel exhibited a morphology that was characterized by clusters of saucer-shaped pits, and these tended to merge into large pits with time. Some of the cold-worked samples exhibited 'tracking' along the highly stressed parts of the specimen loop.

(5) Pits in the ferritic steel were found to be oval in shape and aligned in rows. In general, the pits were deeper than those measured in the austenitic steel.

(6) Analysis of the corrosion products in the pits indicated high levels of Cl, S, Cr, Ni, and Mn species, suggesting that these were involved in the pitting processes.

References

1. Asphahani, A.I., and Silence. (1987). Chapt. 2. In *Metals handbook*, 9th ed., ASM Metals Park, Ohio, vol. 13, p. 113.
2. Colombier, L. (1981). *Molybdenum in stainless steels and alloys*. Climax Molybdenum Company Monograph, p. 9.
3. Sedriks, J. (1979). *Corrosion of stainless steels*. Corrosion Monograph Series, p. 1.
4. Hoar, T.P., and Jacob, R.W. (1967). Breakdown of passivity of stainless steels by halide ions. *Nature*, vol. 216, p. 1299.
5. Bond, A.P., and Lizlous, E.A. (1968). Anodic polarization of austenitic stainless steels in chloride media. *J. Electrochem. Soc.*, vol. 115, p. 1130.

6. Pessal, N., and Liu, C. (1971). Determination of critical pitting potentials of stainless steels in aqueous chloride environments. *Electrochem. Acta*, vol. 16, p. 1987.

7. Wilde, B.E. (1972). A critical appraisal of some popular laboratory electrochemical tests for predicting the localized corrosion resistance of stainless steels in sea water. *Corrosion*, vol. 28, p. 283.

8. Pessal, N., and Nurminen, J.I. (1974). Development of ferritic stainless steels for use in desalination plants. *Corrosion*, vol. 30, p. 381.

9. Sugimoto, K., and Sawada, Y. (1976). The role of alloyed molybdenum in austenitic stainless steels in the inhibition of pitting in neutral halide solutions. *Corrosion*, vol. 32, p. 347.

10. Roy, D.N. (1979). Electrochemical aspects of pitting corrosion of stainless steels in chloride media. *Indian J. Technology*, vol. 17, p. 304.

11. Stefec, R., Franz, F., and Holacek, A. (1979). Influence of heat treatment on pitting corrosion of austenitic Cr–Ni–Mo steels in chloride solutions. *Werkstoffe und Korrosion*, vol. 30, p. 189.

12. Stefec, R., and Franz, F. (1978). A study of the pitting corrosion of cold-worked stainless steels. *Corrosion Science*, vol. 18, p. 161.

13. Kruger, J. (1976). Chemical breakdown of passivity. Passivity and its breakdown on iron and iron base alloys. *USA–Japan Seminar*. Staehle, R.W., and Okada H. (eds). Houston, NACE, p. 91.